International Journal of Refrigeration 149 (2023) 155–167

Contents lists available at ScienceDirect

International Journal of Refrigeration

journal homepage: www.elsevier.com/locate/ijrefrig

Analysis of the characteristics of the gas–liquid mixed artificial snow-making

Analyse des caractéristiques de la production artificielle de neige à partir de mélanges gaz-liquide

Bin Liu [a,b,*], Hengxiang Hu [a,b], Lisen Bi [a,b], Panagiotis E. Theodorakis [c]

[a] *Tianjin Key Laboratory of Refrigeration Technology, Tianjin University of Commerce, Tianjin, 300134, China*
[b] *International Centre in Fundamental and Engineering Thermophysics, Tianjin University of Commerce, Tianjin, 300134, China*
[c] *Institute of Physics, Polish Academy of Sciences, Al. Lotników 32/46, Warsaw, 02-668, Poland*

A R T I C L E I N F O

Keywords:
Evaporation
Cooling
Water droplet
Snow-making

Mots clés:
Évaporation
Refroidissement
Gouttelette d'eau
Neige artificielle

A B S T R A C T

This study investigates the heat and mass transfer of liquid droplets freezing in the process of artificial snow-making, and emphatically analyses the effects of droplet size, ambient temperature and relative humidity on the evaporative cooling and freezing of liquid droplets by establishing a theoretical model. On this basis, the critical droplet size for snow-making under different environmental conditions is obtained, and the accuracy of the droplet freezing model was verified by artificial snow-making experiments. Finally, by analyzing the density of artificial snow under different environmental conditions, the optimum gas-liquid mixing mass ratio (*GLR*) suitable for snow-making is obtained. The results show that the liquid droplets could be frozen under the action of self-evaporation and convection heat transfer with ambient. The time required for the droplet to be frozen completely shows a positive correlation with ambient temperature, relative humidity and droplet size. In the evaporation cooling stage, the droplet cooling rate increases with the decrease of ambient temperature, and in the phase transition stage, the time for the droplet resists the latent heat of phase transition increases with the increase of the droplet size. When the droplet size is smaller than the critical size for snow-making, the artificial snow can be achieved at a maximum temperature of 3 °C. The snow density decreases with the increase of *GLR*. And when the *GLR* is greater than 0.15, the snow density tends to be stable.

1. Introduction

Skiing has become a popular sport as the economy has grown. However, the subsequent increase in the demand for the snowfall cannot be satisfied, due to the insufficiency and frequent fluctuation of the snowfall in nature, which calls for a need to develop the artificial snow-making create artificial snow. Many researchers have undertaken a substantial number of studies on snowflakes, which are mainly focused on three aspects. The first aspect is the impact of snow distribution on the ecosystem, biodiversity, and natural catastrophes (Catherine et al., 2013; Roy et al., 2010; Hoshino et al., 2010; Takeuchi, 2013). The second aspect is the physical qualities of snow such as density, viscosity, water content, porosity, structure, and so on (Lemmetyinen et al., 2016; Brun et al., 2013), as well as optical properties such as reflectivity (Dadic et al., 2008; Tanikawa et al., 2002; Xie et al., 2006). The latter aspect is related to the properties of snow crystals, such as their nucleation and polymerization under various conditions (Liao and Ng, 1990; Zepeda et al., 2001). Artificial snow-making is commonly realized in four ways: (1) snow-making with compressed air, where water flows through the nozzle and breaks down into small droplets, which are subsequently cooled and consolidated in the surrounding air to form snowflakes; (2) snow-making with high pressure water, where water under increased pressure is misted into small droplets by the atomizing nozzle and then these droplets are blown into the surrounding air to form snowflakes; (3) snow-making with the cut ice, in which the ice blocks are scraped with blades to make very thin ice sheets; (4) the ultrasonic technology is used to atomize droplets to form ice crystal, which are combined with droplets again to promote the growth of ice crystals

* Corresponding author.
E-mail address: lbtjcu@tjcu.edu.cn (B. Liu).

https://doi.org/10.1016/j.ijrefrig.2022.12.025
Received 1 October 2022; Received in revised form 21 December 2022; Accepted 24 December 2022
Available online 28 December 2022

and eventually form snowflakes (Yamamoto, 1994).

Both of the first two methods of artificial snow-making use atomized water, and a distinction between them depends on whether compressed air is used. When compressed air is not used to assist the artificial snow-making, the atomization needs to be completed by one-way flow nozzle precipitation, which differs from two-phase flow air-assisted nozzles in its weaker atomization effect and higher water consumption. In contrast, when the compressed air is used for the artificial snow-making, it is necessary to use the two-phase flow nozzles to atomize water, which transforms the water into tiny droplets after being violently disturbed by the compressed air in the mixing chamber inside the nozzle. After the atomization, due to the heat exchange between the tiny water droplets and the ambient cold air, and the heat loss caused by their own evaporation, the tiny water droplets freeze to form the ice crystals. When the cut ice is used for the artificial snow-making, the ice cubes are cut into very thin ice flakes by the ice cutter. The blown flaky snowflakes produced by this method are closer to the natural snowfall, but during the snow-making process a large number of ice cubes are required, which is inconvenient in practical applications. The ultrasonic assisted artificial snow-making technology, which requires the ultrasonic standing wave field to suspend the droplets, is not suitable for outdoor snow-making environment. In addition, although the droplet size produced by ultrasonic spray can be controlled by adjusting the ultrasonic frequency, the ultrasonic technology is mostly used for low-velocity fluids. It appears to be more attractive in various applications such as humidifiers, medical sprayers, spray drying and combustion (Filicicchia, 2012; Briceño-Gutierrez et al., 2015; Peskin Richard and Raco Roland, 1963; Wood and Loomis, 1927).

The nucleation, growth and aggregation of ice crystals have been studied experimentally by several researchers, meanwhile, the molecular dynamics method have been also applied to the study of ice crystal growth (Hallett and Mason, 1958; Bones and Adams, 2009; Carignano et al., 2006). Their study has revealed the kinetics and the time evolution of two freezing systems of pure water and brine. They have also found that the total freezing time of the brine system is longer than that of the pure water. Based on a large amount of data obtained by experiments, Nelson (Nelson, 2001) have established a snow crystal growth prediction model by estimating the diffusion field adjacent to the growing snow crystal and combining various ice crystal growth data. In addition, they have also studied and analyzed the growth process of flat snow crystals and columnar snow crystals under different super saturation at the same temperature below −22 °C. Evans et al. (Evans, 1973) have studied the growth and fragmentation of ice crystals under an electric field and concluded that the growth rate of ice crystals is accelerated in the direction of the electric field.

The droplet freezing process of the artificial snow-making with the atomization by nozzles is similar to the flash evaporation of droplets (Wang et al., 2017). Miyatake et al. (Miyatake et al., 1981) conducted an experimental research on the flash evaporation of the spray occurring in a superheated water jet and have developed an empirical equation for predicting the liquid temperature according to the effects of superheat, flow rate and nozzle diameter on the flash evaporation of the spray. Zhifu et al. (Zhifu et al., 2012) have presented an experimental investigation on the spray and thermal characteristics of flashing spray by using the cryogen R134a. During their experiment, the spray characteristics were measured by the Phase Doppler Particle Analyzer (PDPA), and the experimental results provided a deep understanding into the characteristics of two-phase flashing spray of volatile liquids. Satoh et al. (Satoh et al., 2002) have studied the cooling/freezing process of water droplet evaporation in a vacuum chamber, and the results have shown that the water droplet could be effectively cooled by evaporation, and the cooling rate was dominated by the heat transfer within the droplet. Shin et al. (Shin et al., 2000) have also studied the freezing process of the water sprayed into the vacuum chamber both experimentally and theoretically. Fisenko et al. (Fisenko et al., 2006) conducted an investigation on the cooling process of micron-sized droplets evaporation at low-pressure. They have found that the cooling rate was 2×10^3 K/s with the characteristic time of 1 ms, which was mainly affected by the flow rates of the carrier gas and solution. Cheng et al. (Cheng et al., 2015) have found that the flash evaporation of droplets has a great effect on the heat transfer, which results from their well-established comprehensive mathematical model for the cooling of vacuum flash evaporation.

The basic theory of artificial snow-making is based on the atomization of liquid water into tiny droplets, which subsequently lower their own temperature by heat loss, due to the evaporation and heat transfer with the surrounding environment until they are completely frozen before landing. During the process of the gas-liquid mixed artificial snow-making, not only do both the heat exchange between the droplets flowing out from the nozzle and the environment and the heat loss due to the evaporation of the droplets need to be considered, but also the distribution of droplets in the entire spray field and the environmental conditions, such as temperature and humidity. Although the addition of spoiler can make the snow-making spray field more stable (Li et al., 2022), the size and shape of spoiler may bring inconvenience to the movement of the snow-making machines. In addition to the above parameters, the size of the droplets that directly affects whether they are frozen before landing requires a careful consideration. In a specific ambient temperature and humidity, the freezing ability of the droplets due to the heat loss caused by their own evaporation and the heat transfer between the environment is limited. In this case, in order to achieve a greater degree of droplet freezing, a smaller particle size of the atomization droplet is required. Therefore, it is particularly important to study the critical droplets that can be frozen under different environmental conditions, which will directly determine whether artificial snow-making could be realized.

To summarize, much work have been carried out on snow in terms of natural climatic hazards, the microscopic morphology of ice crystals and the physical properties of snow, but little study has focused on the critical conditions for artificial snow-making based on heat and mass transfer. To this end, in this paper, the heat and mass transfer in the evaporation and freezing processes of a single droplet with different size has been studied, and on this basis, the critical conditions for snow-making under different temperature and humidity were analyzed, which were further verified by artificial snow-making experiments.

2. Experiments and methods

Our study consists of two parts, the simulation of the evaporation and freezing processes of a single droplet and experiments of artificial snow-making. The simulation of the evaporation and freezing process of a single droplet is carried out by establishing a mathematical model through COMSOL software, which is based on the analysis of heat and mass transfer in the evaporation and freezing processes of the droplet by Wang *et al.* and Shin et al. (Wang et al., 2017; Shin et al., 2000). In the artificial snow-making experiment, by intuitively observing whether snow-making can be achieved under different conditions, the critical snow-making condition based on mathematical model is further verified. At the same time, under the premise that snow can be made, the relationship between the mixture ratio of different gas-liquid mass and the snow-making density is studied.

2.1. Simulation of evaporative cooling and freezing of the single droplet

2.1.1. Model of the mass transfer

Fick's law is usually used to express mass transfer during the evaporation process of water droplets. Due to the concentration gradient between the droplet surface and the air, continuous evaporation takes places at the surface of droplets. At this point, the mass loss of the droplet is equal to the quantity of evaporation, which can be described by Eq. (1),

$$\dot{m} = -M_w A_w k_c (C_{w,s} - C_{w,\infty}) \tag{1}$$

$$C_{w,\infty} = \frac{p_v}{RT_a} \tag{2}$$

$$C_{w,s} = \frac{p_s(T_w)}{RT_w} \tag{3}$$

where, $\dot{m}$ is the evaporation rate of droplet, g/s; A_W is the surface area of droplet, m^2; M_W is the molecular weight of water, g/mol; $C_{w,s}$, $C_{w,\infty}$are the vapor concentration at the surface of the droplet and in the air, respectively, mol/m^3; T_W and T_a are the temperature of the droplet and the air, respectively, K; p is the local absolute pressure, Pa; R is the universal gas constant, 8.3145 J/(mol·K).

The saturated water vapor pressure in Eq. (3) can be obtained by an empirical formula as follows (Edition, 2001),

$$\ln(p_s) = \frac{c_1}{T} + c_2 + c_3 T + c_4 T^2 + c_5 T^3 + c_6 \ln T \quad T > 273.15\ K \tag{4}$$

where, c_1=5800.2206, K; c_2=1.3914993; c_3=0.048640239, K^{-1}; c_4=4.1764768 × 10^{-5}, K^{-2}; c_5=1.4452093 × 10^{-8}, K^{-3}; c_6= 6.5459673.

k_c denotes the mass transfer coefficient, kg/s, which can be obtained from the correlation of Sherwood number as follows (Bird et al., 2002),

$$Sh = \frac{k_c d_w}{D_c} = 2 + 0.6 Re^{\frac{1}{2}} Sc^{\frac{1}{3}} \tag{5}$$

$$Sc = \frac{\nu}{D_c} \tag{6}$$

$$Re = \frac{\rho_w d_w u_d}{\mu} \tag{7}$$

where d_W is the diameter of droplet, m; Sc is the Schmidt number; Re is the Reynolds number; Dc is the diffusion coefficient of water vapor in the air, m^2/s; u_d is the velocity of droplet, m/s.

The mass change of droplet can also be expressed by the change in diameter, which is expressed as,

$$\dot{m} = \frac{1}{2}\pi \rho_w d_w{}^2 \frac{d(d_w)}{dt} \tag{8}$$

According to Eqs. (1) and (8), the diameter change caused by the evaporation is converted into formula (9) as follows,

$$\frac{d(d_w)}{dt} = -\frac{2M_w D_c}{\rho_w d_w} Sh (C_{w,s} - C_{w,\infty}) \tag{9}$$

2.1.2. Model of the heat transfer

When the water droplet diffuses in the cold air, the heat transfer between the droplet and the environment is expressed as follows,

$$c_w m_w \frac{dT_w}{dt} = Q_c + Q_{rad} + Q_L \tag{10}$$

The right side of the equation contains the terms for the sensible heat change in the droplet, i.e. (from left to right), the convective heat transfer (Q_c), the absorption/emission of radiation (Q_{Rad}) on the droplet surface, and the latent heat transfer of evaporation (Q_L).

The convective heat transfer between the droplet and the ambient air is calculated as follows (Whitaker, 1972),

$$Q_c = h_c A_w (T_a - T_w) \tag{11}$$

$$h_c = \frac{\lambda Nu}{d_w} \tag{1}$$

$$Nu = 2 + 0.6 Re^{\frac{1}{2}} Pr^{\frac{1}{3}} \tag{13}$$

where h_c is the convection heat transfer coefficient of the droplet, W/(m^2·K); Nu is the Nusselt number of the droplet, and Pr is the Prandtl number of the air flow.

The absorption/emission of radiation at the droplet surface is calculated in Eq. (14). However, it is not considered in this study, due to the small temperature difference (4–8 °C) between the droplet and the environment.

$$Q_{Rad} = \varepsilon_w \sigma A_w (T_w^4 - T_a^4) \tag{14}$$

The latent heat transfer caused by the evaporation is expressed as follows,

$$Q_L = r_L \frac{dm}{dt} \tag{15}$$

The energy balance relationship Eq. (16) is obtained by combining Eqs. (10)–(15), and the change of droplet diameter over time is taken by Eq. (17) by integrating Eq. (9).

$$\frac{1}{6}\rho_w (d_w)^2 c_w \frac{dT_w}{dt} = \lambda Nu (T_a - T_w) - r_L M_w D_c Sh (C_{w,s} - C_{w,\infty}) \tag{16}$$

$$(d_w)^2 = -\frac{4M_w D_c}{\rho_w} Sh (C_{w,s} - C_{w,\infty}) t + (d_{w,0})^2 \tag{17}$$

By substituting Eq. (17) into Eq. (16), the relationship between the droplet temperature and the other parameters is obtained according to Eq. (18). Therefore, after some parameters are given according to this relation, the range of the remaining variables is obtained.

$$\frac{1}{6}\rho_w c_w \left[\frac{4M_w D_c}{\rho_w} Sh (C_{w,\infty} - C_{w,s}) t + (d_{w,0})^2\right] \frac{dT_w}{dt} = \lambda Nu (T_a - T_w) + M_w D_c Sh (C_{w,\infty} - C_{w,s}) r_L \tag{18}$$

The initial droplet critical size $d_{w,0}$ corresponding to the droplet in the evaporative cooling link is given by Eq. (18). After the droplet has been cooled down by evaporative cooling, the temperature of the droplet from its initial temperature to freezing point, which corresponds to a droplet size $d_{w,1}$, after this, the droplet undergoes a freezing phase transition process. Based on the initial critical size, the effect of the latent heat of phase change on droplet freezing is considered as shown in Eq. (19). Then, the freezing of the droplet at a given time is obtained by combining Eqs. (19)-(23). The specific process of droplet evaporative freezing is shown in Fig. 1.

$$\Delta m r_p = \Delta m_e r_L + h_c A_w (T_a - T_w) \Delta t \tag{19}$$

$$\Delta m_e = \frac{1}{6}\pi \rho_w \left[(d_{w,1})^3 - (d_{w,2})^3\right] \tag{20}$$

$$\Delta m = \frac{1}{6}\pi \rho_w (d_{w,2})^3 \tag{21}$$

$$(d_{w,1})^2 = -\frac{4M_w D_c}{\rho_w} Sh (C_{w,s} - C_{w,\infty}) t + (d_{w,0})^2 \tag{22}$$

$$(d_{w,2})^2 = -\frac{4M_w D_c}{\rho_w} Sh (C_{w,s} - C_{w,\infty}) \Delta t + (d_{w,1})^2 \tag{23}$$

Here, Δm denotes the mass of the frozen droplet, kg; r_p denotes the heat of phase change of freezing, kJ/kg; Δm_e denotes the mass of the droplet which continues to evaporate from freezing point to complete freezing, kg; r_L denotes the latent heat of evaporation, kJ/kg; $d_{w,1}$ denotes the droplet size in the evaporative cooling stage before the freezing phase change stage, m; $d_{w,2}$ denotes the size of the droplet when it is completely frozen, m.

2.1.3. Methods and details of the simulation

The following main assumptions were used in this study to simulate the evaporative cooling and freezing processes of the single droplet: (1)

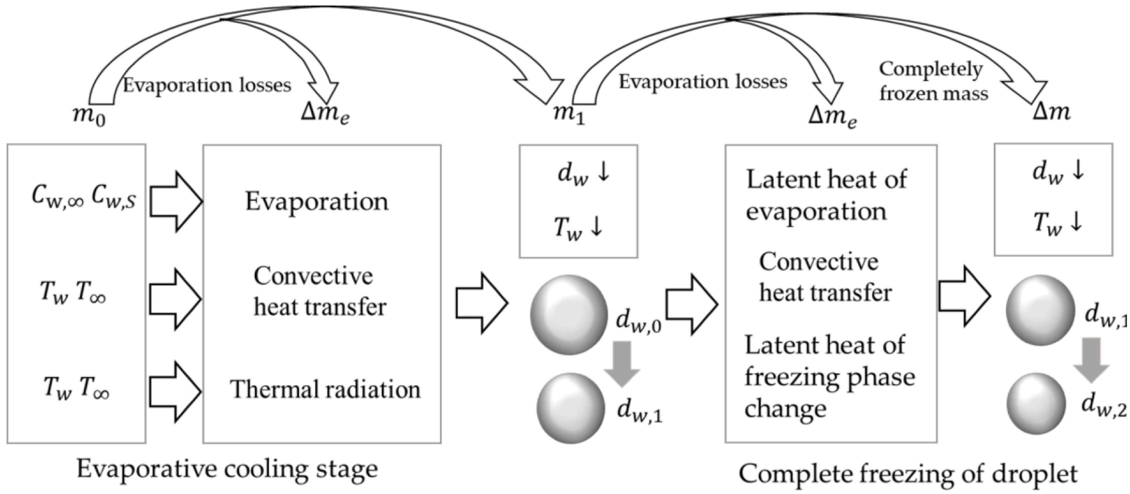

Fig. 1. Schematic diagram of the evaporative freezing process of water drop.

Because the research object is a single droplet, the environmental area is much larger than the single studied droplet area, the evaporation of the droplet leads to a small amount of water vapor entering the environment and does not affect the water vapor concentration of the surrounding environment. Therefore, the effect of single droplet evaporation on the water vapor concentration of the surrounding environment can be ignored (Wang et al., 2017). (2) Although the droplet is not a perfect sphere in the actual evaporation and freezing process, the droplet at the micron level is affected by the surface tension, and the droplet always maintains an approximate sphere. Here we assume that the droplet is a perfect sphere (Beard et al., 2010). (3) Since the droplet size is micron-sized, the maximum temperature difference between the droplet and the environment is only 8 °C, and the heat transfer by radiation is very small, so the radiation between the droplet and the surrounding environment can be ignored.

The determination of mesh independence is an important step in numerical simulation. It is well known that the coordination of numerical analysis results depends on the mesh size. Therefore, it should be shown that the results are independent of the grid in all CFD studies (Selimefendigil et al., 2021; Das¸ et al., 2020). In order to obtain a better grid quality scheme, this study numerically simulated three different grid sizes shown in Fig. 2. Among them, grids 1, 2 and 3 correspond to the number of grids of 77,386, 101,328, 131,476, respectively. By comparing the droplet temperature changes under the conditions of $T_a = -4$ °C and RH = 20%, the best quality grid scheme is obtained. The same overall trend of temperature change is obtained by analyzing different grid schemes. Compared with grid 2 and 3, the maximum temperature offset of grid 1 is 0.7 °C. With the increase of the number of grid units, the results of grid 3 are consistent with those of grid 2, but the calculation time increases with the increase of the number of grids. Therefore, the scheme of grid 2 was adopted to set the grid refinement level of the air domain as normal, and the grid refinement level of the inside of droplet and interface between droplet and air was set to be finer, which ensured the accuracy of the results and reduced the calculation time to a greater extent. In order to make the inside of droplet and interface between droplet and air had better mesh quality, the mesh of the interface between gas and liquid was encrypted. The number and size of the grids in the air domain, the inside of droplet and the droplet-air interface are shown in Table 1. Fig. 3 shows the physical model of the water droplet and the generated mesh.

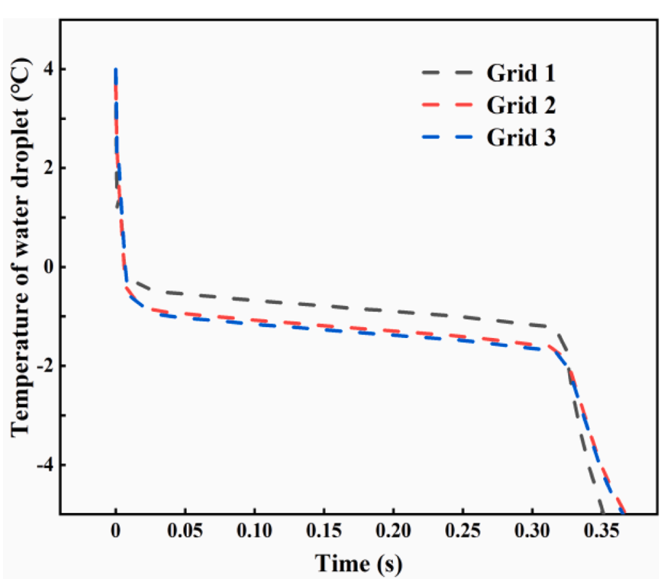

Fig. 2. Grid independence analysis.

COMSOL Multiphysics is used to simulate the cooling and freezing processes of the water droplet. According to the physical phenomena involved in this study, three physical modules were selected, namely laminar flow, dilute material transfer, and fluid heat transfer. For the calculation of the thermophysical properties of the wet air, the fluid heat transfer module in COMSOL was used for the setup (Tsilingiris, 2008), where the initial values of the air domain and droplet parameters were first set and solved by coupling the heat transfer and fluid modules. The equations used for the coupling calculation are as follows,

$$\rho \frac{du}{dt} = \rho F - \nabla P + \mu \nabla^2 u \tag{24}$$

$$\nabla(u) = 0 \tag{25}$$

Table 1
Grid division scheme.

Parameters name	Maximum unit size	Minimum unit size	Curvature factor	Grid Numbers	Mesh quality
The interface between droplet and air	3.7×10^{-5}	4×10^{-6}	0.4	864	0.9063
Inside the droplet	3.7×10^{-5}	4×10^{-6}	0.4	2894	0.6773
Air domain	6.7×10^{-5}	2×10^{-5}	0.6	97,570	0.6591

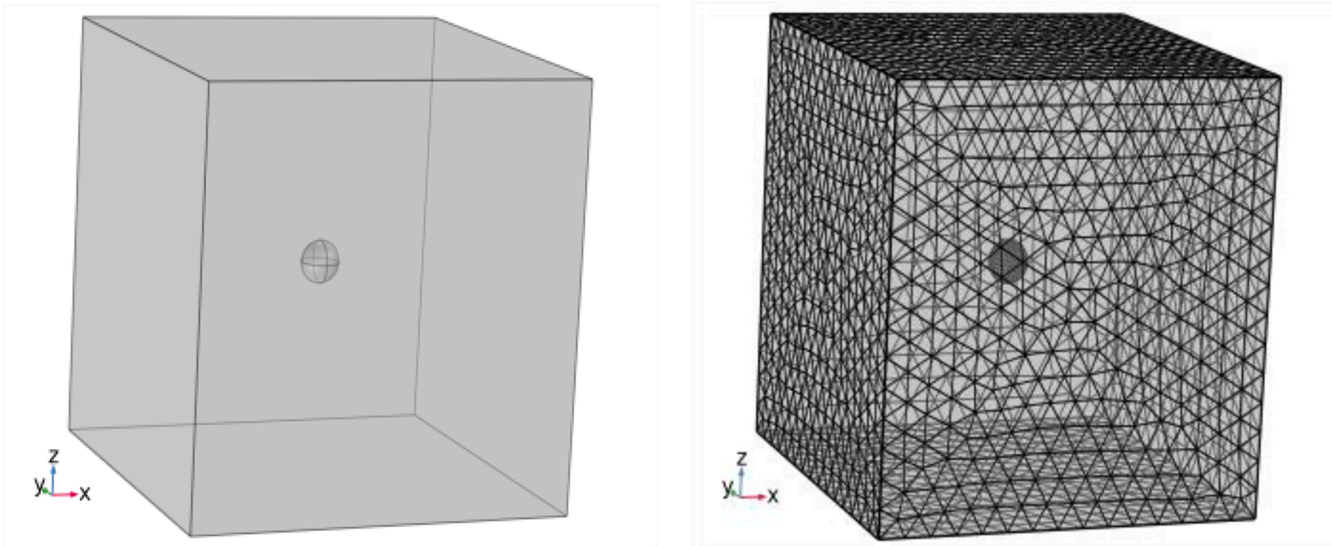

Fig. 3. Physical model of water droplet and mesh. (a) Physical model of one water droplet; (b) Mesh generated by COMSOL.

$$\frac{\partial c}{\partial t} + \nabla\cdot(-D_c\nabla c) + u\cdot\nabla c = R \tag{26}$$

$$\rho_g C_p\frac{\partial T}{\partial t} + \rho C_p u\cdot\nabla T + \nabla\cdot q = Q \tag{27}$$

$$q = -\lambda\nabla\cdot T \tag{28}$$

$$\rho = \theta_1\rho_1 + \theta_2\rho_2 \tag{29}$$

$$C_p = \frac{1}{\rho}\left(\theta_1\rho_1 C_{p,1} + \theta_2\rho_2 C_{p,2}\right) + L_{1\to2}\frac{\partial\alpha_m}{\partial T} \tag{30}$$

$$\alpha_m = \frac{1}{2}\frac{\theta_2\rho_2 - \theta_1\rho_1}{\theta_1\rho_1 + \theta_2\rho_2} \tag{31}$$

$$k = \theta_1 k_1 + \theta_2 k_2 \tag{32}$$

$$\theta_1 + \theta_2 = 1 \tag{33}$$

The boundary conditions of inlet and outlet in the simulation are as follows:

The inlet boundary conditions,

$$u = const \tag{34}$$

$$T_0 = const \tag{35}$$

The outlet boundary conditions,

$$-n\cdot q = 0 \tag{36}$$

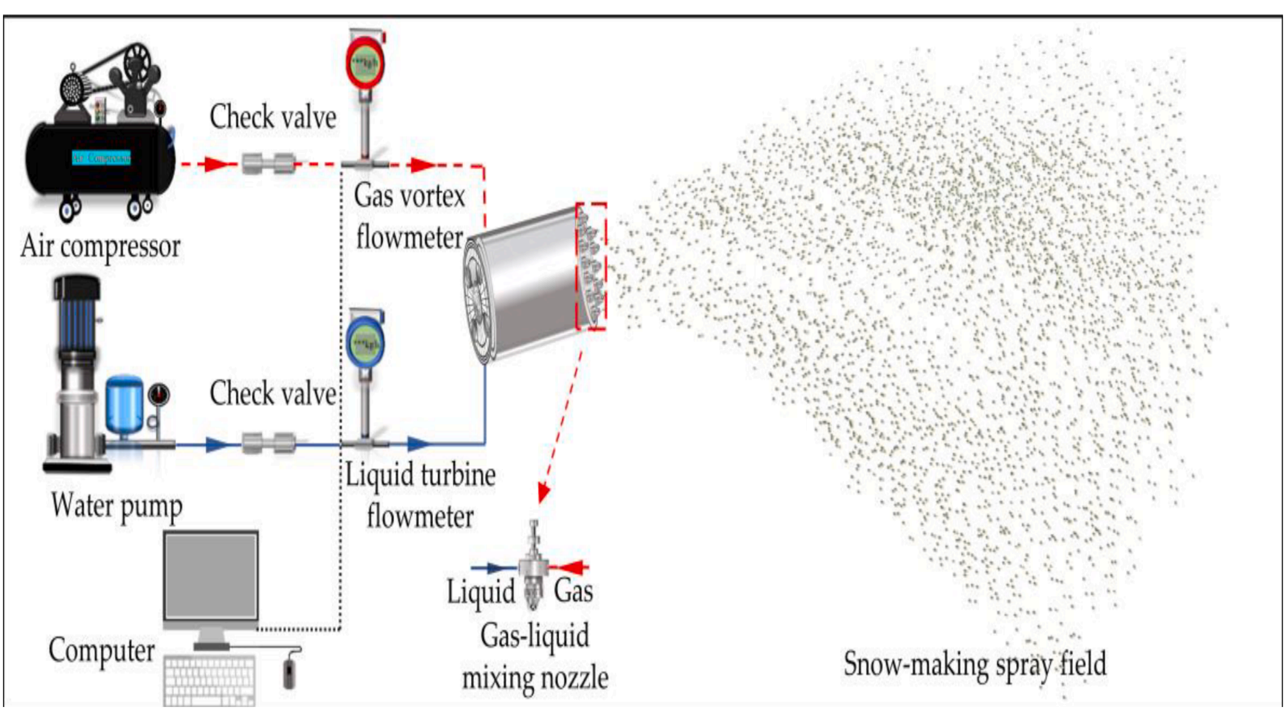

Fig. 4. Schematic diagram of the experimental setup.

$$-n \cdot D_c \cdot \nabla c = 0 \quad (37)$$

Here, ρ is fluid density, kg/m^3, u is fluid velocity, m/s, F is force, N, μ is dynamic viscosity, m^2/s, c is concentration, mol/m^3, D_c is diffusion coefficient, m^2/s, R is gas constant, J/(mol·K), ρ_g is air density, kg/m^3, C_p is fluid constant pressure heat capacity, kJ/(kg·K), λ is air thermal conductivity, W/(m·K), α_m is mass fraction, k_1, k_2 is thermal conductivity, W/(m·K), ρ_1, ρ_2 is the density of liquid phase and solid phase, kg/m^3.

2.2. The experiment of artificial snow-making

The schematic diagram of the experimental device is shown in Fig. 4, including the aerodynamic part, the hydrodynamic part, the data acquisition part and the snow making nozzle. The artificial snow-making nozzle uses the gas–liquid mixed atomization method to manufacture tiny droplets, the size of droplets after atomization is closely related to the mixing state of gas-liquid two-phase fluid in the nozzle cavity. Therefore, the gas-liquid mass mixing ratio is set as the variable. In the internal mixing chamber of the nozzle, the compressed air was mixed with the liquid and tiny bubbles of gas were formed during the mixing process. In the mixture, the tiny bubbles expanded and the liquid broken up into flakes, strips and tiny droplets at the outlet, thus the atomisation effect was achieved (Sovani et al., 2001; Davanlou et al., 2015). The gas expansion leaded to the lower outlet temperature. If the ambient temperature was low, the water drop near the nozzle was easy to freeze, so the insulation cotton and electric heating were used on the pipeline and around the nozzle to prevent the icing phenomenon on the nozzle and pipeline. The nozzle structure is shown in Fig. 5.

On the premise that snow can be made, the influence of gas-liquid mixing ratio on snow-making was studied. The premise condition of the snow-making was obtained by numerical simulation and verified by snow-making experiments. Finally, the snow density of snow making was analyzed by comparing different gas-liquid mass mixing ratio, and the best gas-liquid mass ratio was obtained.

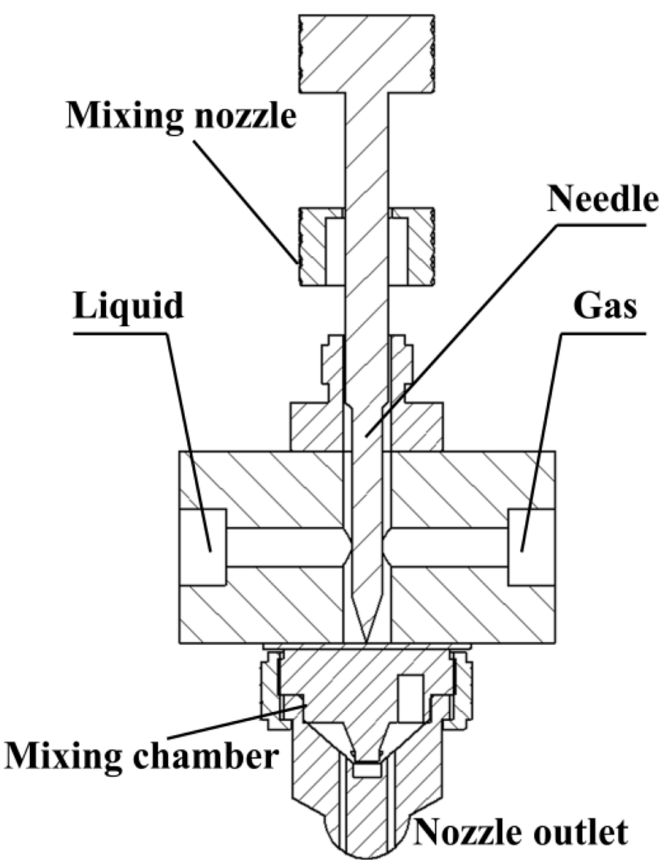

Fig. 5. The structure of mixing nozzle.

When the gas and liquid entered the mixing chamber of the gas–liquid mixing nozzle, the mixing and shredding processes of gas and liquid affected the quality of the first-level atomization (Matouš et al., 2017; Moon et al., 2020). In addition, the mixing ratio of gas and liquid shown in Eq. (38) directly affected the particle size of droplets in the spray field.

$$GLR = \frac{q_{m,a}}{q_{m,l}} \quad (38)$$

where, the GLR is the ratio of mass mixed gas to liquid, $q_{m,a}$ is the mass flow of compressed air, kg/s, and $q_{m,l}$ is the mass flow of water, kg/s.

The experiments were carried out under the conditions of compressed air pressure of 0.6 MPa and ambient humidity of 25±5%, and the effects of the ambient temperature, gas–liquid mixing ratio (GLR), and snowfall distance on the density of artificial snow were studied in the experiments. The calculation formula of snow density is shown in Eq. (39). The phenomenon of water or gas pouring occurs when the pressure difference between the gas pipeline and the liquid pipeline of the gas–liquid mixing nozzle is larger than the maximum permitted pressure difference of nozzles. When the air pressure exceeds the hydraulic pressure, the gas reverses into the liquid pipeline, obstructing the flow of water. So, in extreme instances, gas can block the liquid stream. A similar phenomenon occurs when the liquid pressure exceeds the gas pressure. In order to avoid this phenomenon, the gas and liquid pipeline were firstly open, and then the liquid (gas) pipeline pressure were increased or decreased. The pressure sensor with accuracy of 0.065%, which was installed in front of the inlet of the nozzle gas and liquid pipeline, was used to accurately record the gas and liquid pressure. By observing the gas-liquid pressure difference between the water pouring and the air pouring, the maximum allowable pressure difference of the gas-liquid internal mixing nozzle of 0.3 MPa was obtained.

$$\rho_s = \frac{\sum_{i=1}^{10} M_i}{10mnh_x} \quad (39)$$

where, ρ_s is the snow density, kg/m^3, M_i is the mass of the snow samples measured each time, kg. m and n are the side length of the snow samples, m, and h_x is the height of the snow samples, m.

3. Results and discussion

3.1. Evaporative freezing time of water droplets

Fig. 6 shows the temperature variation of water droplets at different ambient temperatures. As the ambient temperature decreases, the time required for the water droplets to be cooled from 4 °C to −5 °C shortens significantly. The droplet temperature changes can be divided into three stages according to the temperature behavior: rapid evaporative cooling of first stage, phase transition phase of second stage, refreezing and cooling phase of third stage. In the first stage, the evaporative cooling rate of the droplet increases with the decrease of ambient temperature, and as the droplet temperature decreases, the phase transition occurs in the second stage. During the stage of the freezing phase transition, the temperature of droplets is nearly constant due to the interaction between the latent heat generated by the freezing of the droplet and the heat transfer caused by the convection and evaporation. At this point the constant temperature maintained by the droplets is known as the freezing point. When the heat loss caused by the convection and evaporation is more than the latent heat generated by the freezing, the temperature is no longer constant and continues to drop in the third stage. Moreover, when the convective heat transfer and evaporation are stronger, the generation of latent heat by freezing phase transition only weakens, but the latter effect cannot stop the drop in droplet

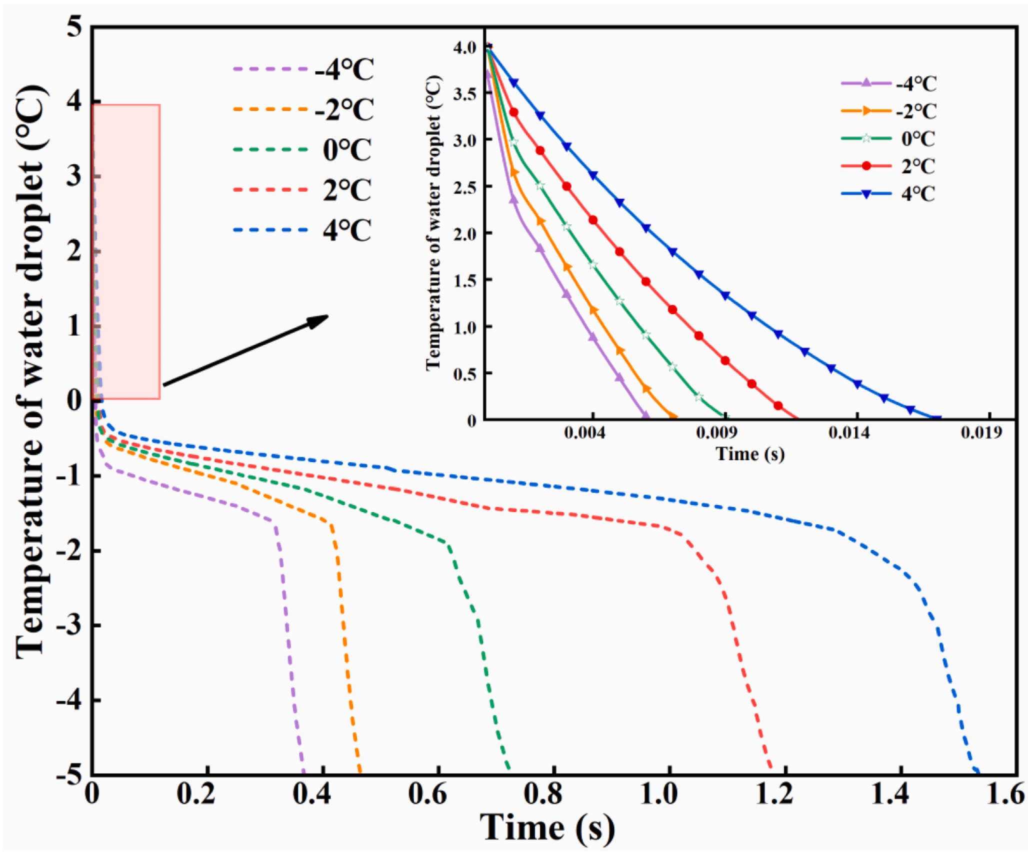

Fig. 6. Evaporative freezing time of water droplets at different ambient temperatures (the relative humidity: 20%, Initial droplet temperature: 4 °C, air speed: 2 m/s, initial diameter: 100 μm).

temperature. After the latent heat of the freezing phase transition of the droplet is offset, the temperature of the droplet continues to decrease due to convection and evaporation, but the rate is smaller compared to the initial evaporation stage (Shin et al., 2000; Kim et al., 2001).

With the increase of ambient temperature, the heat transfer between the droplet and the environment is limited, the time required to transfer the latent heat by the droplet during the freezing is prolonged. As a result, it takes longer time for the droplets to reach the freezing state. At the ambient relative humidity of 20% and ambient temperatures of −4 °C and 4 °C, the time required for the droplets to reach −5 °C is 0.368 s and 1.52 s, respectively. Fig. 7 shows the phase transition process of the droplet at different times, with the initial state of liquid phase (1) and eventually reaching the solid phase (0). In comparison with rapid evaporative cooling stage and refreezing and cooling phase stage, the

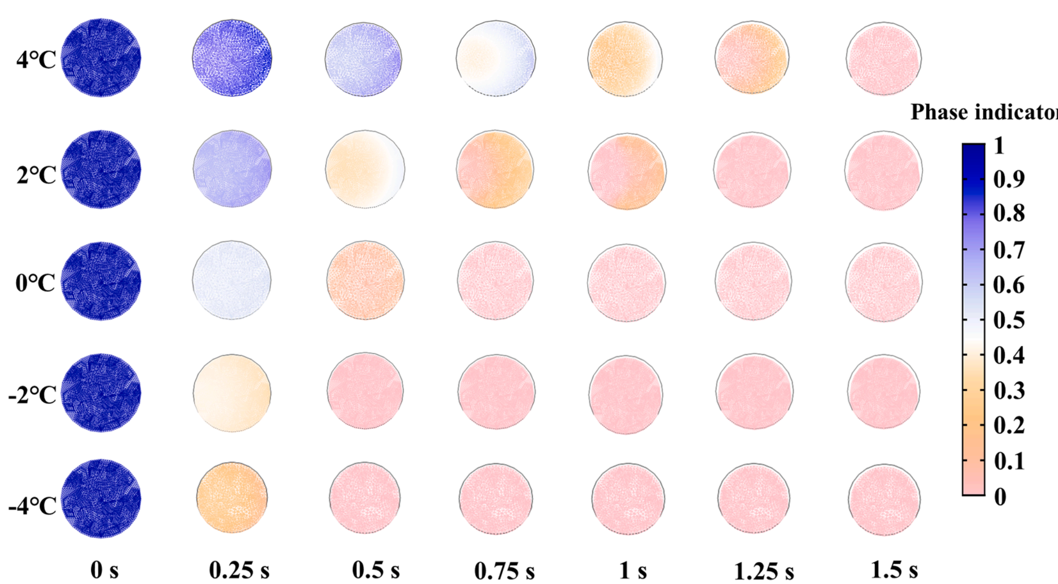

Fig. 7. Phase transition state of droplets at different ambient temperatures versus time (the relative humidity: 20%, initial droplet temperature: 4 °C, air speed: 2 m/s, initial diameter: 100 μm).

phase transition stage of the droplet takes the longest time, and the boundary of liquid–solid transition obviously changes with time. In particular, with the decrease of ambient temperature, the time required for the phase transition stage becomes shorter, whereas the solid proportion of droplets at the same time obviously becomes larger. When the ambient temperature is 2 °C and −4 °C, the time interval for the droplets to freeze into the solid state is 1.25 – 1.5 s and 0.5 – 0.75 s. Afterwards, the phase state of the droplets does not change with time. Through the above analysis of the temperature variations and phase variations of the droplets, the feasibility of artificial snow-making under theoretical conditions for different environmental conditions can be determined theoretically.

The diameter of droplet is also an important factor to be considered in the artificial snow-making, due to it is negatively correlated with the specific surface area of droplet, which directly affects the heat and mass transfer between the droplet and the environment. Under the same ambient temperature and humidity, the temperature variation of droplets with different diameters over time are consistent with the results of

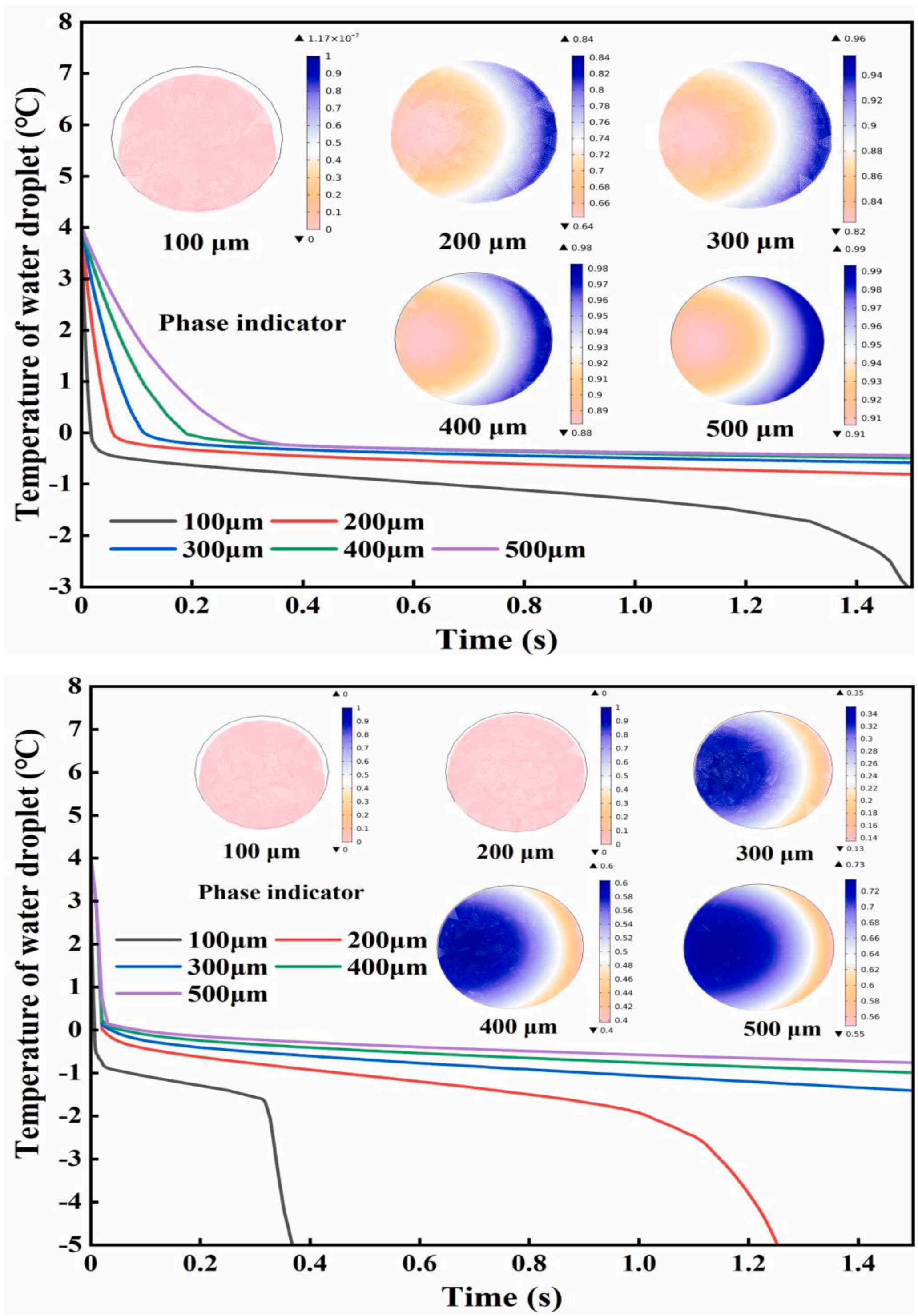

Fig. 8. Changes of temperature and phase transition during the evaporative freezing of droplet with different diameters (The ambient temperatures of a and b are 4 °C and −4 °C, and the relative humidity is 20%, the initial temperature of the droplet is 4 °C).

B.S. Kim et al. (Shin et al., 2000; Kim et al., 2001) as shown in Fig. 8. When the ambient temperature is 4 °C and the time is 1.5 s, only the droplets with the diameter of 100 μm undergo complete phase transition, the coexistence phenomenon of ice and water is shown in the droplets with other diameters, the percentage thresholds of liquid phase for droplets with diameters of 200 μm, 300 μm, 400 μm and 500 μm are 0.64 - 0.84, 0.82 - 0.96, 0.88 - 0.98 and 0.91 - 0.99 respectively. In the first stage (evaporative cooling stage), the cooling rate decreases with the increase of diameter, and the temperature in the second stage (phase change stage) all show approximately constant values, but for droplets with the diameter of 100 μm, the temperature still tends to decrease slowly. This is due to the fact that the droplets with smaller diameters have a larger specific surface area, which leads to the more effectively heat transfer with the environment. At this time, the heat released by the phase transition is less than the transferred heat. In contrast, the droplets with larger diameters have the smaller specific surface area but greater mass, the latent heat released by phase transition is greater than the transferred heat, so it takes a longer time to offset this part of latent heat, resulting in the second stage (phase change stage) lasts long enough, as shown in Fig. 8(a).

When the ambient temperature is −4 °C, the diameter of the droplets in which complete freezing occurs also becomes larger, as shown in Fig. 8(b), and the cooling rate of the first stage (evaporative cooling stage) is higher than that of the first stage when the ambient temperature is 4 °C. Only the droplets with diameters of 100 μm and 200 μm undergo the complete phase transition, while the droplets with diameters of 300 μm, 400 μm and 500 μm remain in the ice and water coexistence state, with the percentage thresholds of liquid phase are 0.14–0.34, 0.4–0.6 and 0.55–0.73 at 1.5 s respectively. By comparing Fig. 8(a) and Fig. 8(b), it can be seen that the phase states (proportion of ice water) at the same time are different for the droplets with same diameter under different ambient temperatures. When the diameters of droplet were 300 μm, 400 μm and 500 μm, the threshold values for the percentage of liquid phase in the ice-water coexistence state were reduced by 0.65 ± 0.03, 0.43 ± 0.05 and 0.31 ± 0.05 compared to the ambient temperature of 4 °C. As shown in the phase transition diagrams of the droplet (Fig. 8(a), Fig. 8(b)), the freezing of the droplet develops gradually from the surface to the center (Satoh et al., 2002), and the proportion of the liquid phase in the front is smaller than that in the rear during the flight of the droplets in the state of coexistence of ice and water. Noted that the right side of the droplet is the front side, since the heat transfer of the front end is greater than that of the rear side, the distribution of the phase ratio between the left and right side of the droplet is inconsistent during the flight. In summary, reducing the ambient temperature is obviously the most direct way to make the droplet be frozen completely. However, due to the great uncertainty of environmental factors in actual outdoor snow-making activities, it is necessary to determine the critical size that can be frozen in different environments.

3.2. Critical diameter of droplet for snow-making

According to Eq. (18), the heat and mass transfer processes of water droplet depend on many parameters, such as initial temperature and diameter of droplet, ambient temperature and relative humidity, allowed time for snow-making, *etc*. If a part of these parameters is selected as the constraint conditions for the design of snow-making devices, the feasible region of other parameters can be obtained by Eq. (18). Fig. 9 shows the critical diameter of the droplets frozen by evaporation in the process of spraying at different ambient temperatures and humidity. On this basis, the change of droplet size in the diffusion process before landing was calculated in conjunction with Eqs. (19)-(23), and the possibility of droplet freezing was further analyzed. Fig. 10 shows the mechanism of the freezing phase of the droplet.

After assuming the time of the evaporative cooling, the critical particle size is obtained by the assistance of Eq. (18), as shown in Fig. 9. In the analysis process, the total time for the droplet leaving the nozzle until landing was assumed to be 3 s, and whether the droplet was frozen when it reached the ground was judged by solving the energy conservation equation of the evaporative cooling and the droplet freezing stages. In the droplet freezing stage, when the droplet temperature is lower than the ambient temperature, the freezing phase change heat and convective heat exchange of the droplet would weaken its cooling. At this time, the heat taken away by the evaporation should be greater than the first two, otherwise the droplet cannot cool down to the freezing temperature, as shown in Fig. 10, B1, B2. When the droplet temperature is higher than the ambient temperature, the heat taken away by the convective heat transfer and latent heat of evaporation makes the droplet cool down faster, while the heat of freezing phase change weaken the droplet cooling, and when the cooling amount of first two is greater than the heat of freezing phase change, the droplet would be frozen, as shown in Fig. 10, A1, A2. Another situation is also possible when the droplet temperature is higher than the ambient temperature. After the convective heat transfer and latent heat of evaporation have firstly reduced the droplet temperature below the ambient temperature, the convective heat transfer and heat of freezing phase change weaken the droplet cooling again, and at this point the superimposed process of A1 and B1 is shown in Fig. 10.

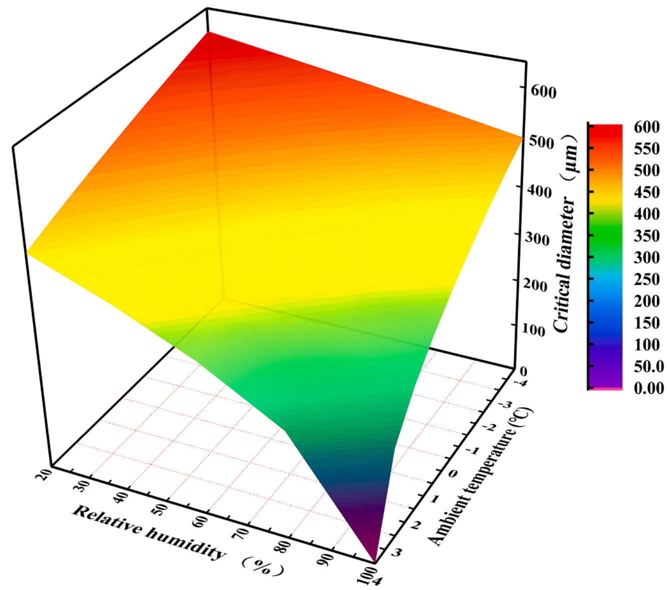

Fig. 9. Critical diameter of water droplets for snow-making.

Fig. 11 shows the critical diameter of the droplet at different relative humidity (Fig. 11(a)) and ambient temperature (Fig. 11(b)). At the same ambient temperature, the critical diameter of droplets for snow-making decreases with the increase of relative humidity, and the higher the ambient temperature, the greater the effect of relative humidity on the critical diameter. At the same relative humidity, the critical diameter of droplets for snow-making decreases with the increasing of ambient temperature, and the decrease trend is more obvious with the increase of relative humidity. The changes in the relative humidity and air temperature affect the strength of droplet evaporative cooling and convection, both of which have a significant effect on the critical diameter of the droplets. When the ambient temperature or relative humidity is higher, the evaporation and convection heat transfer of droplets are limited, so the heat generated by the droplet freezing can not be transferred in time, thus resulting in a smaller critical diameter for snow-making. As a result, snow-making equipment with a high atomisation capacity is required so that the appropriate size of droplets can be produced by equipment according to the ambient temperature and humidity.

For the droplets of the same diameter, the amount of heat loss required for complete freezing is fixed and the source of the heat loss is

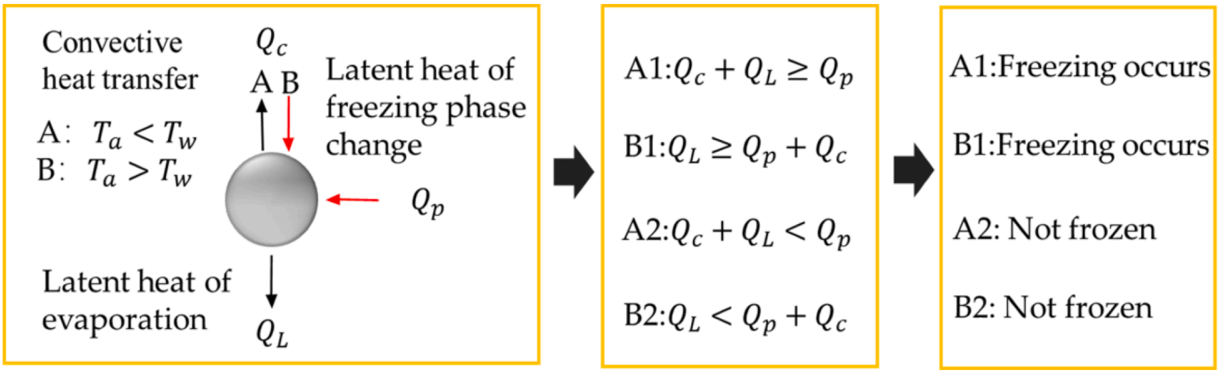

Fig. 10. Diagram of the freeze-phase transition mechanism of water drop.

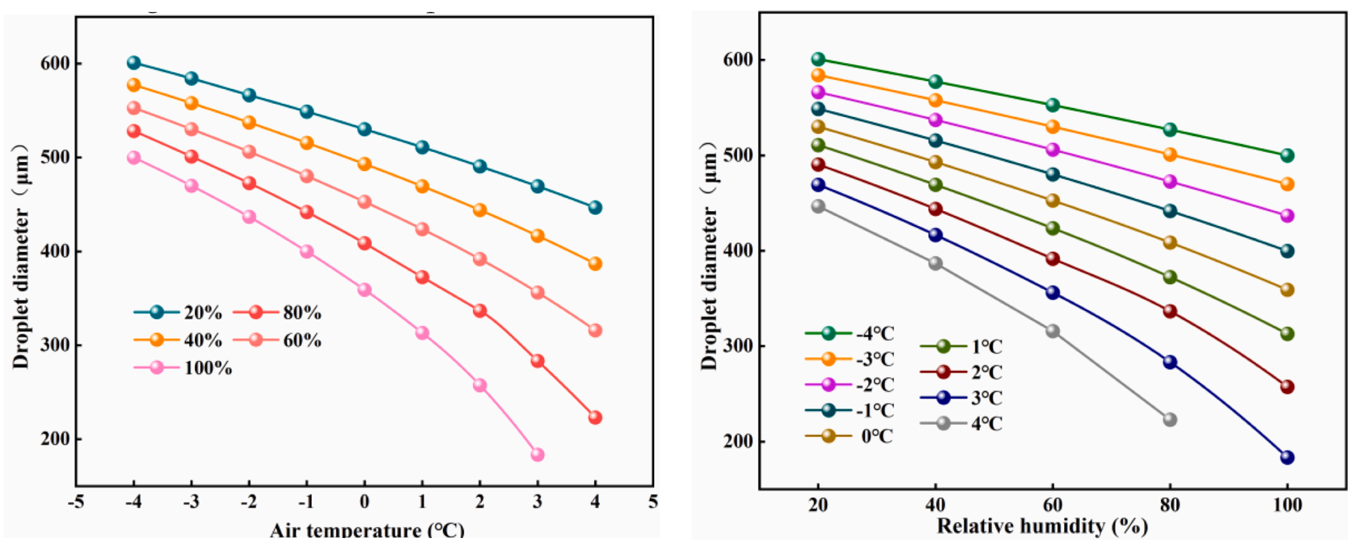

Fig. 11. Critical diameter of the droplet. (a) Critical diameter of the droplet at different relative humidity (b) Critical diameter of the droplet at different ambient temperature.

mainly the convective heat transfer between the droplets and the environment and the self-evaporation of droplets, when the ambient

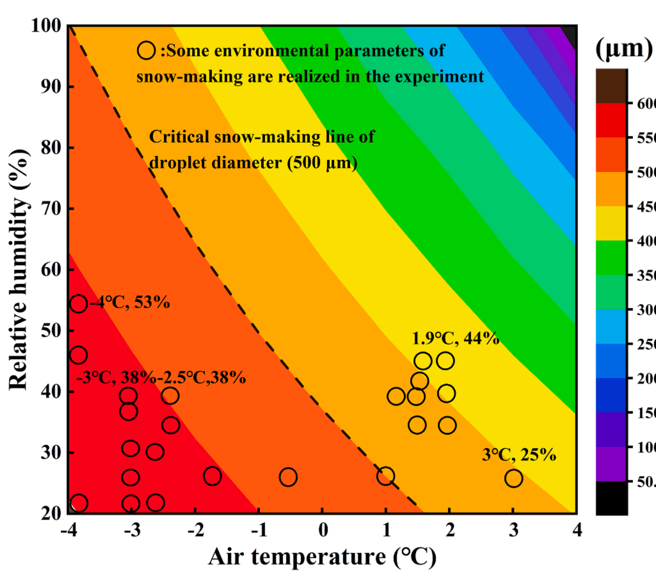

Fig. 12. The verified theoretical threshold value for artificial snow-making at different ambient temperatures and humidity.

temperature is lower, the convective heat transfer between the droplet and the environment is enhanced, so the heat loss demand of the self-evaporation is relatively reduced. In other words, the complete freezing of droplets can be achieved under the relatively low ambient temperatures and high humidity conditions, as shown in Fig. 12 (ambient temperature −4 °C, relative humidity 53%). In contrast, at relatively high ambient temperatures, the complete freezing of droplets can only be achieved by controlling the relative humidity at the low values (ambient temperature 3 °C, relative humidity 25%).

As can be seen from Fig. 12, the artificial snow-making is only achieved in the area below the critical snow line, in which the droplet diameter is 500 μm, the relative humidity is 53% and the ambient temperature is −4 °C, this is due to the fact that there is a critical droplet size for different temperatures and humidity levels, and in the actual snow-making process, once the droplet size is larger than the critical size, the droplets cannot be completely frozen to form snowfall. When the droplet diameter is 500 μm, the critical environmental conditions for that the artificial snow-making can be achieved are shown in Fig. 12. It can be seen that the snow can be made at both low ambient temperatures and high relative humidity (T_a= −4 °C, RH = 53%) and high ambient temperatures and low relative humidity (T_a = 1 °C, RH = 25%). In addition, the low temperature and low humidity environment, which provides a large driving force for droplet evaporation and freezing, is very conducive to artificial snow production. Under the condition of T_a = 3 °C, RH = 25%, we also achieved artificial snow-making, although it exceeded the calculated lower limit of critical temperature and humidity

(T_a = 1 °C, RH = 25%) corresponding to the freezing of droplets (D = 500 μm). This is due to the fact that the droplets formed by atomisation are smaller than 500 μm by adjusting the nozzle gas-liquid mixing state. When the droplet diameter is smaller than the freezable diameter corresponding to the environment, the lower limit of ambient temperature and humidity at which the droplets can be frozen will be further enlarged. However, once the droplet size is larger than the critical size, the droplets cannot be completely frozen to form the snowfall. Therefore, in order to achieve snow-making, it must be carried out in a lower ambient temperature and humidity, otherwise it will lead to snow-making failure. In summary, based on the temperature and humidity corresponding to snow-making, the artificial snow-making can be achieved as long as the droplet size is lower than the critical droplet size, which fully validates the accuracy of the critical droplet size for snow-making.

3.3. Optimal snow-making experimental research based on snow density

In artificial snow-making, the gas-liquid mass mixing ratio is the most direct reaction to gas-liquid mixing state in the mixing chamber of two-phase flow nozzles, which also directly affects the droplet size (Sovani et al., 2001). For the same type of snow-making nozzles, it is necessary to adjust the gas-liquid mixing state (gas-liquid mixing mass ratio) inside the nozzle, so the droplet size is small enough to accelerate the heat transfer from droplet, which results in the form of tiny ice crystals for freezing to obtain high quality artificial snow. Fig. 13 shows the relationship between the density of artificial snow and the gas-liquid mass mixing ratio under different environmental conditions, it can be seen that at different ambient temperatures and air-liquid mass mixing ratios, the snow density decrease with the increase of snowfall distance. There are two reasons for this phenomenon, on the one hand, the size of droplets produced by artificial snow-making machine is uneven, the larger droplets land closer to the snow machine due to the greater flight resistance and gravity. The smaller droplets fly farther and fall farther with the airflow, so the snow is less dense at a distance and the foggy snow can be seen far from the snow-making machine. On the other hand, during the flight process of droplets, the differences in size and flight speed leading to the collision of droplet., When the aerodynamic effect is less than the surface tension, the droplets can not break through the steady state and the droplet aggregation forms, so the droplet size become larger at this time, and the droplet size gradually decreases with the increase of the flight distance, resulting in a gradual decrease in the snow density with the increase of the distance.

The droplet diameter shows a negative correlation with the gas-liquid mixing mass ratio (Sovani et al., 2001; Matouš et al., 2017), which is consistent with the variation of snow density with the gas-liquid mass mixing ratio, as shown in Fig 13(d). It can be seen when the gas-liquid mixing ratio of 0.05, the snow density is 1000 kg/m^3, this is due to the gas-liquid mass mixing ratio is small, the nozzle atomization effect is poor, and the heat loss of droplets caused by self-evaporation

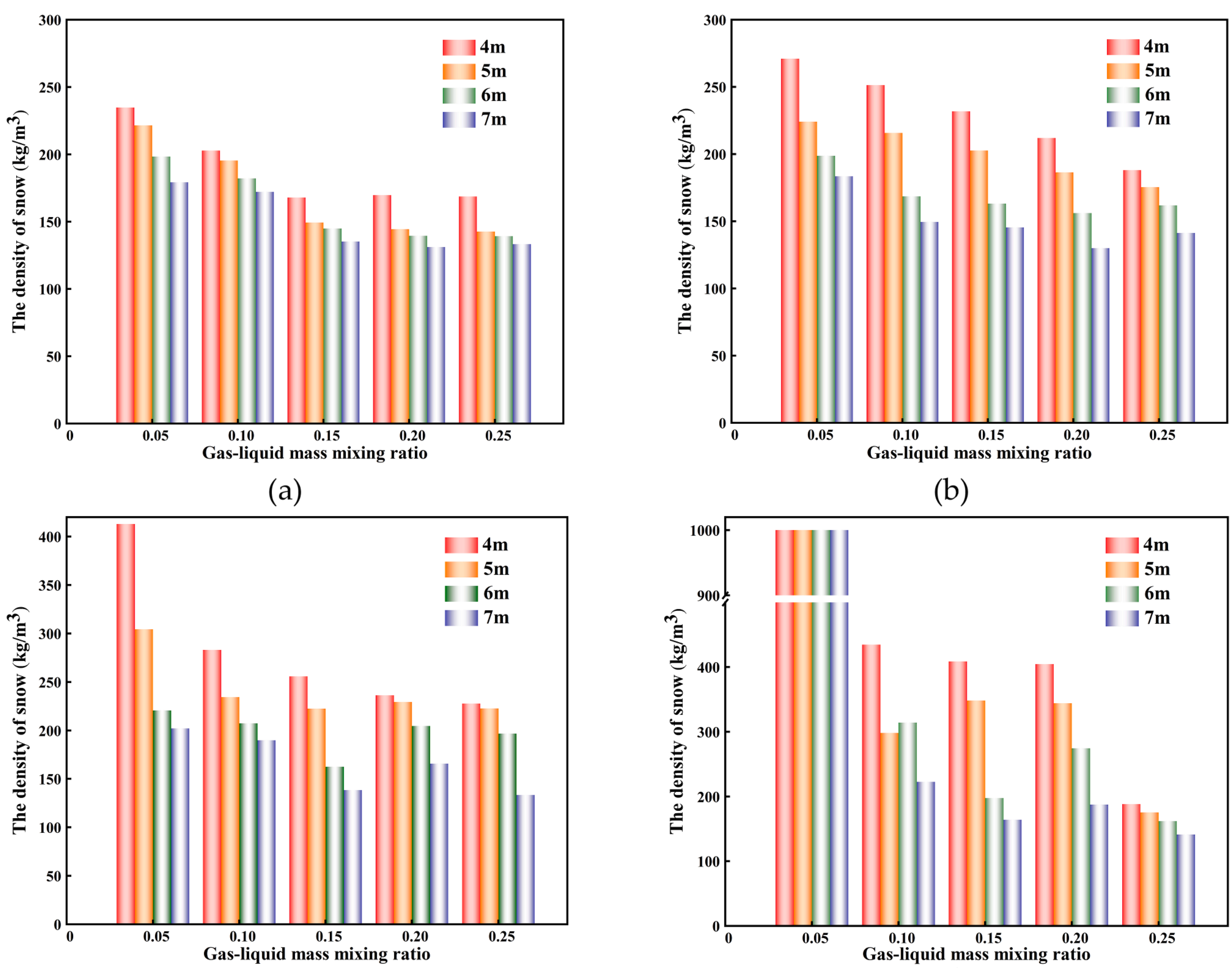

Fig. 13. Variation of snow density with the gas–liquid mixing ratio at different distances (The water temperature is 4 °C, the ambient temperature for a to d is −2 °C, −0.5 °C, 1 °Cand 3 °C, respectively, the relative humidity is 25±5%, and the compressed air pressure is 0.6 Mpa).

and convective heat transfer is limited, so the droplet finally exists in the form of ice and water mixture. In summary, in order to realize artificial snow-making, it is necessary not only to consider the influence of environmental factors on the evaporative cooling and convective heat transfer of the droplets, but also to strictly control the size of the droplets during the process of artificial snow-making.

The mentioned snow density in this paper refers to fresh snow. Which is relatively soft and does not undergo long-term gravity compaction and wind action. The density of fresh snow placed at night will increase with the action of gravity compaction and wind (Vivian et al., 2007; Pomeroy et al., 1998). The ski resort will use the snowcat to compact the fresh snow, or make the fresh snow completely solidified and hardened by placing it for a long time. Combined with the Fig. 13, under the same relative humidity, the higher the ambient temperature, the greater the snow density value. When the ambient temperature is lower than 0 °C ($T_a = -0.5$ °C, −2 °C), the maximum snow density is 300 kg/m^3. When the ambient temperature is higher than 0 °C ($T_a = 1$ °C, 3 °C), the maximum snow density is 413 kg/m^3. From the perspective of improving snow-making quality and saving energy, in order to make more liquid droplets could be frozen into ice crystals to form snowfall under the condition that the temperature and humidity satisfies the snow-making requirements. When the snow-making ambient temperature is enough low, the *GLR* can be set to 0.05. On the contrary, when artificial snow is made above 0 °C, if the *GLR* is greater than 0.15, the density of snow tends to be stable with the increase of *GLR*. Therefore, the *GLR* of 0.15 can be used as a reference value, and *GLR* can be gradually reduced in combination with snow density. Note that when *GLR* is small ($GLR = 0.05$, $T_a = 3$ °C), snow and water coexistence occurs. Therefore, when the ambient temperature is enough low, the *GLR* less than 0.10 is appropriate, which corresponds to higher snow density.

4. Conclusions

In this study, the evaporative cooling and freezing phase transition processes of a single water droplet, which are considered as the first and second stage of artificial snow-making are investigated. The effects of relative humidity, ambient temperature, initial diameter on the freezing of water droplets is analyzed in detail. Moreover, the appropriate range of parameters for artificial snow-making is obtained. At the same time, the optimum air-liquid mass mixing ratio suitable for artificial snow-making is also obtained. The main conclusions are summarized as follows:

(1) The maximum diameter of water droplets allowed for artificial snow-making increases with the decrease of ambient temperature and relative humidity. Through the droplet phase transition process and droplet cooling curve, we have found that the droplet can be frozen when the relative humidity and the diameter of water droplets are limited within the suitable ranges.
(2) During the cooling and freezing processes, the trend of temperature change of water droplet is almost the same. In particular, with the increase of ambient temperature, the cooling time of water droplets increases. The relative humidity has a greater effect on the cooling of droplets than ambient temperature.
(3) The snow density increases with the decrease of *GLR* under the premise that snow can be made. The *GLR* is 0.05 corresponds to higher snow density. The overall snow density at ambient temperatures above 0 °C is greater than that below 0 °C. When *GLR* is greater than 0.15, the snow density tends to be stable.

Declaration of Competing Interest

The authors declare that they have no known competing financial interests or personal relationships that could have appeared to influence the work reported in this paper.

Acknowledgements

This work was financially supported by the Integrated Projects utilizing the Space Environment on ISS and CSS supported by CMSA and ESA (TGMTYY00-RW-03).

References

Bird, R.B., Steawart, W.E., Lightfoot, E.N., 2002. Transport Phenomena, 2nd edition. John Wiley and Sons, New York.
Bones, J., Adams, E.E., 2009. Controlling Crystal Habit in a Small Scale Snowmaker. International Snow Science Workshop, Davos.
Briceño-Gutierrez, D., Salinas-Barrera, V., Vargas-Hernández, Y., et al., 2015. On the ultrasonic atomization of liquids. Phys. Procedia 63, 37–41. https://doi.org/10.1016/j.phpro.2015.03.006.
Brun, E., Vionnet, V., Boone, A., et al., 2013. Simulation of Northern eurasian local snow depth, mass, and density using a detailed snowpack model and meteorological reanalyses. J. Hydrometeorol. 14 (1), 203–219. https://doi.org/10.1175/jhm-D-12-012.1.
Carignano, M.A., Baskaran, E., Shepson, P.B., et al., 2006. Molecular dynamics simulation of ice growth from supercooled pure water and from salt solution. Ann. Glaciol. 44 (1), 113–117. https://doi.org/10.3189/172756406781811646.
Catherine, L., Aurélien, D., Vogel, T.M., 2013. The dynamic arctic snow pack: an unexplored environment for microbial diversity and activity. Biol.-Basel 2 (1), 317–330. https://doi.org/10.3390/biology2010317.
Cheng, W.l., Chen, H., Hu, L., Zhang, W.w., 2015. Effect of droplet flash evaporation on vacuum flash evaporation cooling: modeling. Int. J. Heat Mass Transf. 84, 149–157. https://doi.org/10.1016/j.ijheatmasstransfer.2014.12.078.
Dadic, R., Schneebeli, M., Lehning, M., Hutterli, M.A., Ohmura, A., 2008. Impact of the microstructure of snow on its temperature: a model validation with measurements from Summit, Greenland. J. Geophys, Res. Atmos. 113 (D14) https://doi.org/10.1029/2007JD009562.
Das¸, M., Alıç, E., Akpinar, E.Kavak, 2020. Numerical and experimental analysis of heat and mass transfer in the drying process of the solar drying system. Eng. Sci. Technol. an Int. J. 24, 236–246. https://doi.org/10.1016/j.jestch.2020.10.003.
Davanlou, A., Lee, J.D., Basu, S., et al., 2015. Effect of viscosity and surface tension on breakup and coalescence of bicomponent sprays. Chem. Eng. Sci. 131, 243–255. https://doi.org/10.1016/j.ces.2015.03.057.
Evans, L.F., 1973. The growth and fragmentation of ice crystals in an electric field. J. Atmos. Sci. 30 (8), 1657–1664. https://doi.org/10.1175/1520-0469(1973)030<1657:TGAFOI>2.0.CO;2.
Filicicchia, Daniel J., 2012. Ultrasonic Atomizing Nozzle With Variable Fan-Spray Feature. Patent 8297530, U.S.
Fisenko, S.P., Wang, W.-N., Wuled Lenggoro, I., Okyuama, K., 2006. Evaporative cooling of micron-sized droplets in a low-pressure aerosol reactor. Chem. Eng. Sci. 61 (18), 6029–6034. https://doi.org/10.1016/j.ces.2006.05.028.
Edition, Handbook A F.SI, 2001. American Society of Heating. Refrigeration and Air-Conditioning Engineers, Atlanta, USA.
Hallett, J., Mason, B.J., 1958. The influence of temperature and supersaturation on the habit of ice crystals grown from the vapour. P. Roy. Soc. Lond a Mat. 247 (1251), 440–453. https://www.jstor.org/stable/100632.
Hoshino, T., Terami, F., Tkachenko, O., Tojo, M., Matsumoto, N., 2010. Mycelial growth of the snow mold fungus, Sclerotinia borealis, improved at low water potentials: an adaption to frozen environment. Mycoscience 51 (2), 98–103. https://doi.org/10.1007/S10267-009-0013-3.
Beard, Kenneth V., Bringi, V.N., Thurai, M., 2010. A new understanding of raindrop shape. Atmos. Res. 97, 396–415. https://doi.org/10.1016/j.atmosres.2010.02.001.
Kim, B.S., Shin, H.T., Lee, Y.P., et al., 2001. Study on ice slurry production by water spray. Int. J. Refrig. 24 (2), 176–184. https://doi.org/10.1016/S0140-7007(00)00013-X.
Lemmetyinen, J., Schwank, M., Rautiainen, K., et al., 2016. Snow density and ground permittivity retrieved from L-band radiometry: application to experimental data. Remote Sens. Environ. 180, 377–391. https://doi.org/10.1016/j.rse.2016.02.002.
Li, Z., Zhang, T., Chen, Y., Wang, Z., 2022. The effect of continuous trapezoidal straight spoiler plates on the vortex-induced vibration of wind turbine towers. Atmosphere (Basel) 3 (13), 447. https://doi.org/10.3390/atmos13030447.
Liao, J.C., Ng, K.C., 1990. Effect of ice nucleators on snow making and spray freezing. Ind. Eng. Chem. Res. 29 (3), 361–366. https://doi.org/10.1021/ie00099a010.
Matouš, Z., Lukas, W., Milan, M., 2017. Low-pressure twin-fluid atomization: effect of mixing process on spray formation. Int. J. Multiph. Flow 89, 277–289. https://doi.org/10.1016/j.ijmultiphaseflow.2016.10.015.
Miyatake, O., Tomimura, T., Ide, Y., Fujii, T., 1981. An experimental study of spray flash evaporation. Desalination 36 (2), 113–128. https://doi.org/10.1016/S0011-9164(00)88635-X.
Moon, S., Huang, W., Wang, J., 2020. Spray formation mechanism of diverging-tapered-hole GDI injector and its potentials for GDI engine applications. Fuel 270, 117519. https://doi.org/10.1016/j.fuel.2020.117519.
Nelson, Jon., 2001. Growth mechanisms to explain the primary and secondary habits of snow crystals. Philos. Mag. A 81 (10), 2337–2373. https://doi.org/10.1080/01418610108217152.
Peskin Richard, L., Raco Roland, J, 1963. Ultrasonic atomization of liquids. J. Acoust. Soc. Am. 9 (35), 1378–1381. https://doi.org/10.1121/1.1918700.
Pomeroy, J.W., Gray, D.M., Shook, K.R., et al., 1998. An evaluation of snow accumulation and ablation processes for land surface modelling. Hydrol. Processes

12 (5), 2339–2367. https://doi.org/10.1002/(SICI)1099-1085(199812)12:15<2339::AID-HYP800>3.0.CO;2-L.

Roy, A., Royer, A., Turcotte, R., 2010. Improvement of springtime streamflow simulations in a boreal environment by incorporating snow-covered area derived from remote sensing data. J. Hydrol. 390 (1), 35–44. https://doi.org/10.1016/j.jhydrol.2010.06.027.

Satoh, I., Fushinobu, K., Hashimoto, Y., 2002. Freezing of a water droplet due to evaporation—Heat transfer dominating the evaporation–freezing phenomena and the effect of boiling on freezing characteristics. Int. J. Refrig. 25 (2), 226–234. https://doi.org/10.1016/S0140-7007(01)00083-4.

Selimefendigil, F., Coban, S.O., Oztop, H.F., 2021. Numerical analysis of heat and mass transfer of a moving porous moist object in a two-dimensional channel. Int. Commun. Heat Mass Transf. 121. https://doi.org/10.1016/j.icheatmasstransfer.2020.105093.

Shin, H.T., Lee, Y.P., Jurng, J., 2000. Spherical-shaped ice particle production by spraying water in a vacuum chamber. Appl. Therm. Eng. 20 (5), 439–454. https://doi.org/10.1016/S1359-4311(99)00035-6.

Sovani, S.D., Sojka, P.E., Lefebvre, A.H., 2001. Effervescent atomization. Prog. Energ. Combust. Sci. 27 (4), 483–521. https://doi.org/10.1016/S0360-1285(00)00029-0.

Takeuchi, N., 2013. Seasonal and altitudinal variations in snow algal communities on an Alaskan glacier (Gulkana glacier in the Alaska range). Environ. Res. Lett. 8 (3), 1345–1346. https://doi.org/10.1088/1748-9326/8/3/035002.

Tanikawa, T., Aoki, T., Nishio, F., 2002. Remote sensing of snow grain-size and impurities from airborne multispectral scanner data using a snow bidirectional reflectance distribution function model. Ann. Glaciol. 34, 74–80. https://doi.org/10.3189/172756402781817437.

Tsilingiris, P.T, 2008. Thermophysical and transport properties of humid air at temperature range between 0 and 100°C. Energy Convers. Manag. 49 (5), 1098–1110. https://doi.org/10.1016/j.enconman.2007.09.015.

Vivian, M., Bernt, L., Karl, V.H., Kim, R.L., 2007. Predicting snow density using meteorological data. Meteorol. Appl. 14 (4), 413–423. https://doi.org/10.1002/met.40.

Wang, C., Xu, R., Song, Y., Jiang, P., 2017. Study on water droplet flash evaporation in vacuum spray cooling. Int. J. Heat Mass Transf. 112, 279–288. https://doi.org/10.1016/j.ijheatmasstransfer.2017.04.111.

Whitaker, S., 1972. Forced convection heat transfer correlations for flow in pipes, past flat plates, single cylinders, single spheres, and for flow in packed beds and tube bundles. AIChE J 18 (2), 361–371. https://doi.org/10.1002/aic.690180219.

Wood, R.W., Loomis, A L.XXXVIII, 1927. The physical and biological effects of high-frequency sound-waves of great intensity. Philos. Mag. 4 (22), 417–436. https://doi.org/10.1080/14786440908564348.

Xie, Y., Yang, P., Gao, B.C., Kattawar, G.W., Mishchenko, M.I., 2006. Effect of ice crystal shape and effective size on snow bidirectional reflectance. J. Quant. Spectrosc. Radiat. Transf. 100 (1), 457–469. https://doi.org/10.1016/j.jqsrt.2005.11.056.

Yamamoto, Yasuo., 1994. Method and Apparatus For Making Snow, 5301512. U.S. Patent.

Zepeda, S., Yin, Y., Orme, C.A., 2001. Atomic force microscope chamber for in situ studies of ice. Rev. Sci. Instrum. 72 (11), 4159–4163. https://doi.org/10.1063/1.1406933.

Zhifu, Z., Weitao, W., Bin, C., Guoxiang, W., Liejin, G., 2012. An experimental study on the spray and thermal characteristics of R134a two-phase flashing spray. Int. J. Heat Mass Transf. 55 (15/16), 4460–4468. https://doi.org/10.1016/j.ijheatmasstransfer.2012.04.021.